THE ASTROPHYSICAL JOURNAL, 469:648–661, 1996 October 1

SPECTROSCOPIC MONITORING OF ACTIVE GALACTIC NUCLEI FROM CTIO. II. IC 4329A, ESO 141−G55, ARAKELIAN 120, AND FAIRALL 9

CLÁUDIA WINGE,[1,2] BRADLEY M. PETERSON,[3] MIRIANI G. PASTORIZA,[1] AND THAISA STORCHI-BERGMANN[1]
Received 1995 December 28; accepted 1996 April 19

ABSTRACT

The results of an intensive monitoring campaign on the Seyfert 1 galaxies IC 4329A and ESO 141−G55 are presented. Variability was detected in both continuum and broad emission line fluxes, and the cross-correlation analysis indicates that the most likely delay between the variations of the 6225 Å continuum and the response of the Hβ and Hα emission lines for IC 4329A is ∼15–25 days. For ESO 141−G55, the time-series analysis was inconclusive, and we could not obtain a clear cross-correlation signal between the lines and continuum light curves. We also present new data obtained for AKN 120 and Fairall 9, consisting of two sets of optical spectra taken ∼4 months apart. Both objects underwent not only significant flux variability (by up to a factor of ∼2) in this interval but also strong Hα and Hβ profile variations.

Subject headings: galaxies: active — galaxies: individual (IC 4329A, ESO 141−G55, Arakelian 120, Fairall 9) — galaxies: Seyfert

1. INTRODUCTION

Continuum and emission-line variability is a well-known characteristic of Seyfert 1 and quasar nuclei (see Peterson 1988, 1993 for reviews). In the standard model for these active galactic nuclei (AGNs), the continuum from an unresolved central source ionizes the high-velocity gas of the surrounding broad-line region (BLR), thus producing the broad (up to a few times 10^4 km s^{-1}) component of the permitted emission lines. Fluctuations in the ionizing continuum will therefore appear in the emission-line fluxes delayed by an amount comparable to the light-travel time from the central source to the emission region. Simultaneous monitoring of the continuum and emission lines could, in principle, provide information about the structure, size, and kinematics of the BLR gas by using reverberation mapping techniques (Blandford & McKee 1982). Within the last few years, intensive monitoring campaigns have provided data with the necessary time resolution and coverage for quantitative time-series analysis (Clavel et al. 1991; Dietrich et al. 1993, 1994; Erkens et al. 1995; Jackson et al. 1992; Korista et al. 1995; Maoz et al. 1990, 1991; Peterson et al. 1991, 1992, 1993, 1994; Reichert et al. 1994; Salamanca et al. 1994; Stirpe et al. 1994a, 1994b; Wanders et al. 1993).

During the period 1991 December–1992 July, in parallel with the observations for the NGC 3783 AGN Watch campaign (Stirpe et al. 1994b), we carried out an intensive spectroscopic monitoring campaign at Cerro Tololo Inter-American Observatory (CTIO) on a few other Seyfert galaxies of different luminosities. The results for NGC 3227 have already been published (Winge et al. 1995, hereafter Paper I), and in this paper, we present the data and results for the monitoring of two southern AGNs, IC 4329A and ESO 141−G55, as well as the less well sampled data obtained for the higher luminosity objects AKN 120 and Fairall 9.

The Seyfert 1 nucleus of IC 4329A was detected by Disney (1973) and presents an optical spectrum characterized by strong internal reddening [$E(B-V) \approx 0.8$ mag; Marziani, Calvani, & Sulentic 1992; but see Winkler et al. 1992] and very broad permitted lines with double-peaked profiles (Pastoriza 1979; Wilson & Penston 1979). The host is a late-type lenticular galaxy, seen almost edge-on. A dust lane is visually evident along the disk, and there is evidence of interaction with a nearby companion, IC 4329, a giant elliptical galaxy (Unger et al. 1987; Giuricin, Mardirossian, & Mezzetti 1990). The optical light shows significant polarization oriented parallel to the dust lane (Martin et al. 1982), suggesting the presence of a magnetic field in the plane of the galaxy, but there also appears to be an additional polarized component, which can be associated with dust scattering in a torus surrounding the AGN (Wolstencroft et al. 1995) or with a nonthermal process like electron scattering or synchrotron emission (Brindle et al. 1990). The AGN in IC 4329A is an X-ray source (Cooke et al. 1978; Elvis et al. 1978; Delvaille, Geller, & Schnopper 1978; Zdziarski et al. 1994) with a conflicting history of variability detection (Marshall, Warwick, & Pounds 1981; Tennant & Mushotzky 1983; Petre et al. 1984; Fabian et al. 1993). Photometric and spectrophotometric studies in the optical spectrum evidence the presence of variability in the continuum (Hamuy & Maza 1987; Winkler et al. 1992) and in the broad emission lines (Morris & Ward 1988; Marziani et al. 1992; Winkler 1992).

The AGN in ESO 141−G55 is a bright but not very well studied source. It was identified as Seyfert 1 by Elvis et al. (1978) from the X-ray *Ariel 5* survey list of Cooke et al. (1978) and confirmed as such by Ward et al. (1978). High-resolution spectra of the Balmer lines (Rafanelli 1985; Stirpe 1990) show that the line profiles are asymmetric and that the Balmer decrement is a function of velocity, being greater at the wings than at the line core. There are inconclusive reports of variability in the X-ray bands (Marshall et al. 1981; Tennant & Mushotzky 1983), and optical and UV

[1] Departamento de Astronomia, Instituto de Física, Universidade Federal do Rio Grande do Sul, Avenida Bento Gonçalves 9500, C.P. 15051, CEP 91501-970 Porto Alegre, RS, Brazil; winge@if.ufrgs.br.

[2] Visiting Astronomer, Cerro Tololo Inter-American Observatory of the National Optical Astronomy Observatories, operated by AURA, Inc., under contract with the National Science Foundation.

[3] Department of Astronomy, Ohio State University, 174 W. 18th Avenue, Columbus, OH 43210.

TABLE 1

IC 4329A AND ESO 141−G55 OBSERVING LOGS

JD (2,440,000+)	UT Date (1992)	IC 4329A			ESO 141−G55		
		Air Mass	Scaling Factors	Comments	Air Mass	Scaling Factors	Comments
8643	Jan 21	1.19	1.00		...	...	
8647	Jan 25	1.06	1.34		...	...	
8651	Jan 29	1.06	1.03		...	...	
8656	Feb 3	1.02	0.92		...	...	
8660	Feb 7	1.01	0.85	Cirrus	...	...	
8664	Feb 11	1.00	0.87		...	...	
8668	Feb 15	1.01	1.33	Clouds	...	...	
8676	Feb 23	1.06	1.39		...	...	
8677	Feb 24	1.01	1.04		...	...	
8678	Feb 25	1.07	0.87		...	...	
8704	Mar 22	1.18	1.14		1.46	0.78	
8712	Mar 30	1.11	0.97		1.53	0.97	
8716	Apr 3	...	...		1.40	1.33	
8720	Apr 7	1.05	1.01		1.36	0.96	
8724	Apr 11	1.09	0.93		1.53	0.93	
8728	Apr 15	1.10	0.85	Clouds	1.51	1.36	Clouds
8732	Apr 19	1.06	1.01		1.67	0.66	Cirrus
8736	Apr 23	1.06	0.87		1.48	0.96	
8752	May 9	1.03	1.38		1.19	1.00	
8764	May 21	1.02	1.04		1.17	0.83	Cirrus
8772	May 29	...	...		1.27	2.14	Cirrus
8776	Jun 2	1.03	0.88		1.18	0.90	
8783	Jun 9	...	...		1.14	0.63	
8794	Jun 20	1.34	0.90		1.15	1.03	
8802	Jun 28	...	...		1.16	0.89	
8804	Jun 30	...	...		1.14	0.59	
8808	Jul 4	1.12	1.86		1.14	0.98	
8810	Jul 6	...	...		1.14	1.48	
8812	Jul 8	...	...		1.16	1.05	
8814	Jul 10	...	...		1.15	0.81	Clouds
8818	Jul 14	1.64	1.11		...	...	
8822	Jul 18	1.26	1.03		1.14	0.93	
8824	Jul 20	1.27	1.14		1.14	1.04	
8826	Jul 22	1.42	1.78		1.15	1.23	Cirrus
8830	Jul 26	1.34	0.89		1.14	0.97	
8832	Jul 28	1.50	0.79		1.26	1.02	

TABLE 2

ARAKELIAN 120 AND FAIRALL 9 OBSERVING LOGS

JD (2,440,000+)	UT Date	AKN 120			Fairall 9		
		Air Mass	Scaling Factors	Comments	Air Mass	Scaling Factors	Comments
8607	1991 Dec 16	...	...	Clouds	1.18	0.82	Clouds
8619	1991 Dec 28	1.19	1.10	Clouds	1.32	1.31	
8623	1992 Jan 1	1.16	0.78		1.35	1.12	
8627	1992 Jan 5	1.16	0.96		1.31	0.87	
8631	1992 Jan 9	1.16	0.64	Cirrus	1.36	0.94	Cirrus
8635	1992 Jan 13	1.27	0.70		1.36	0.98	
8643	1992 Jan 21	1.15	0.87		...	...	
8647	1992 Jan 25	1.16	0.78		...	...	
8651	1992 Jan 29	1.16	0.66		...	...	
8656	1992 Feb 3	1.21	0.69		...	...	
8660	1992 Feb 7	1.19	1.04		...	...	
8664	1992 Feb 11	1.22	1.13		...	...	
8668	1992 Feb 15	1.26	1.09		...	...	
8672	1992 Feb 19	1.18	0.84		...	...	
8676	1992 Feb 23	1.19	0.75		...	...	
8678	1992 Feb 25	1.19	0.72		...	...	
8808	1992 Jul 4	...	...		1.15	0.92	
8822	1992 Jul 18	...	...		1.14	1.06	
8824	1992 Jul 20	...	...		1.16	1.05	
8830	1992 Jul 26	1.84	1.28		1.14	0.80	
8832	1992 Jul 28	1.77	0.92		1.14	0.96	
8834	1992 Jul 30	1.73	1.00		1.14	1.00	

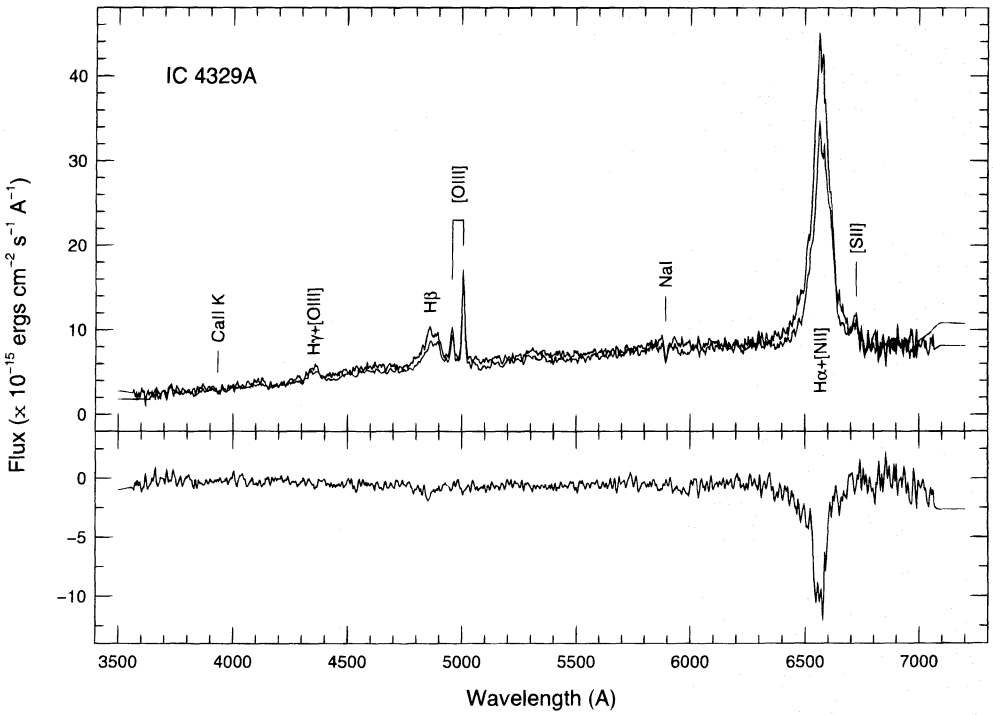

FIG. 1.—*Top*: Representative spectra of IC 4329A obtained during the monitoring: JD 2,448,643 (*upper spectrum*) and 2,448,736 (*lower spectrum*). *Bottom*: The difference spectrum.

variability has been reported by Chapman, Geller, & Huchra (1985), Morris & Ward (1988), Winkler et al. (1992), and Winkler (1992). Using data from the *IUE* archives, Koratkar & Gaskell (1991) analyzed the UV continuum and emission-line light curves using cross-correlation techniques and obtained lags of ~30 and ~90 lt-days between the variations of the UV continuum and the response of the Lyα and C IV λ1549 lines, respectively.

The continuum and emission lines of AKN 120 have a widely discussed history of flux and line-profile variability (see Lyutyi 1976; Foltz et al. 1981; Kollatschny et al. 1981; Peterson et al. 1985; Alloin, Boisson, & Pelat 1988; Peterson, Korista, & Wagner 1989; Marziani et al. 1992). The broad-line profiles are complex, with double or even triple peaks of variable relative intensity (Korista 1992) and a strong red shoulder attributed to a blend of Fe II multi-

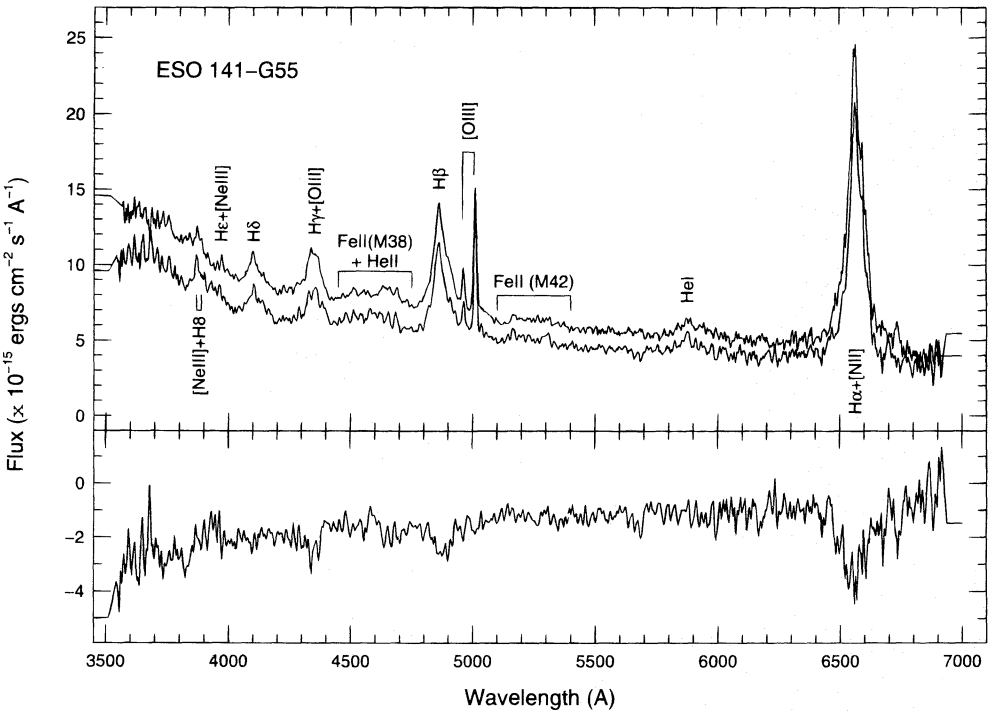

FIG. 2.—Same as Fig. 1, but for ESO 141 – G55. *Top*: JD 2,448,716 (*upper spectrum*) and 2,448,732 (*lower spectrum*).

plets and a possibly "broad" component of the [O III] lines (Meyers & Peterson 1985). The response of the emission lines to the continuum variability has been studied in a systematic way for several years (see Peterson & Gaskell 1991 and references therein), but the results are not conclusive. The time delay derived from the optical continuum and Hβ light curves indicates a BLR radius of $\sim$40 lt-days, much smaller than the size predicted by the ionization models. Koratkar & Gaskell (1991) obtained a similar value using the *IUE* database. A larger value for the emission-line region's radius cannot, however, be dismissed, because of the nonuniformity of the data sampling and the irregularity of the variability behavior.

Fairall 9 has been known as a variable source since its identification as an AGN (Fairall 1977). The X-ray spectrum is variable in flux and shape (Morini et al. 1986). In the UV, this object shows a "saturation limit" in the relationship of C IV λ1549 with the continuum (Wamsteker & Colina 1986; Shields, Ferland, & Peterson 1995) that suggests the presence of an optically thin broad-line component. The time delay between the UV continuum variations and the emission lines' response implies a BLR radius between 150 and 200 lt-days (Koratkar & Gaskell 1991). The UV and optical continua are found to vary in phase, but the near-infrared emission, which is emitted by dust warmed by the central continuum source, is delayed by $\sim$400 days (Clavel, Wamsteker, & Glass 1989; Lub & de Ruiter 1992; Barvainis 1992).

2. OBSERVATIONS

The data were obtained with the CTIO 1.0 m telescope and Cassegrain spectrograph plus "2D-FRUTTI" detector during the period 1991 December 16–1992 July 30. The instrumental setup was the same for all the observations, with a 5″ slit oriented east-west and spectral coverage from 3500 to 7200 Å. The resolution is 8 Å, measured from the FWHM of the comparison lines. The two-dimensional spectrograms were reduced according to IRAF standard procedures, and one-dimensional spectra were extracted in a 10″ window centered on the maximum of the continuum emission. The large slit width and extraction windows were employed to avoid, as much as possible, seeing and differential refraction effects. The spectra were flux-calibrated using the standard spectrophotometric stars from Stone & Baldwin (1983), which were observed with a 10″ slit. The observing logs are presented in Tables 1 and 2, and Figures 1 and 2 show examples of the spectral variations observed for IC 4329A and ESO 141−G55, respectively, during this campaign.

3. ANALYSIS OF THE DATA

3.1. *Relative Scaling of the Spectra*

As is common in variability studies, relative flux calibration of the spectra has been accomplished by assuming that the flux in the narrow emission lines was constant over the duration of the monitoring. The absence of extended [O III] emission at levels that could cause aperture effects was verified from inspection of the original two-dimensional spectrograms. The spectra for each object studied here were internally calibrated using a variant of the method described by van Groningen & Wanders (1992). The program finds the optimum flux-scaling factor, wavelength shift, and convolution factor for each spectrum of a data set (with respect to a reference spectrum) by varying these parameters until the residuals of one or more narrow lines in the difference between the two spectra are minimized. For all objects studied in this paper, the residuals of [O III] λ5007 were minimized. The reference spectra and [O III] λ5007 normalization fluxes are listed in Table 3. The accuracy of the internal calibration, as judged from the [O III] λ5007 residuals, is within 5% for all objects except AKN 120, for which the normalization procedure is not very stable as a result of the small equivalent width of [O III] λ5007 and the possibly variable underlying feature produced by Fe II multiplets and the red wing of Hβ. In this case, the normalization of each spectrum was checked by integrating by hand the [O III] λ5007 flux above a local continuum defined by a smooth interpolation of the underlying line profile, and small adjustments (always less than 10%) were made to the flux scaling. Table 2 lists the final values of the scaling factors for this object.

Since all spectra were obtained with the same instrument and setup, the convolution factor has almost no effect on the results in this case. All data were corrected for Galactic reddening [IC 4329A, $E(B-V) = 0.033$; ESO 141−G55, $E(B-V) = 0.047$; AKN 120, $E(B-V) = 0.093$; Fairall 9, $E(B-V) = 0.0$; Burstein & Heiles 1984] and redshift, as measured by using the strongest narrow emission lines in each spectrum. Flux scales and integrated flux measurements, however, have not been transformed to the rest frames of the objects.

3.2. *Derivation of the Light Curves*

All the observed spectra are contaminated to some extent by the underlying stellar population, which has the effect of diluting the continuum variations through the presence of a constant component. For each of the objects studied in this paper, we assessed the contribution of starlight to the nuclear spectra by examining the diluted equivalent widths of stellar absorption features in a high signal-to-noise ratio (S/N) spectrum obtained by averaging the best individual observations (i.e., excluding the ones with lower S/N due to poor weather) of IC 4329A and ESO 141−G55 and the spectra of the two sets of data of AKN 120 and Fairall 9. The mean spectra clearly reveal the presence of the Ca II K λ3933 and Mg I+Mg *h* λ5175 absorption lines in IC 4329A and in the low state of Fairall 9, defined by the average of the JD 2,448,808–2,448,834 observations.

By measuring the equivalent width of an absorption feature that arises from the stellar population in the nuclear spectrum of an AGN and comparing it with the equivalent width of the same feature in a normal galaxy of similar morphological type and luminosity, or in the bulge of the AGN's host galaxy, it is possible to evaluate the fraction of the continuum at the wavelength of the absorption lines in the AGN's nuclear spectrum that arises from the underlying

TABLE 3

REFERENCE SPECTRUM AND [O III] λ5007 NORMALIZATION FLUX

Object	JD (2,440,000+)	UT Date (1992)	F([O III] λ5007) (10^{-15} ergs cm^{-2} s^{-1})
IC 4329A	8643	Jan 21	186.5 ± 22.5
ESO 141−G55...	8752	May 9	139.2 ± 9.7
AKN 120	8834	Jul 30	70.1 ± 17.4
Fairall 9.....	8834	Jul 30	164.2 ± 14.9

TABLE 4

LINE AND CONTINUUM INTEGRATION WAVELENGTH WINDOWS

Component	Wavelength Window (Å)	Interpolated Continuum Window (Å)
IC 4329A		
F_λ(4210 Å)	4172–4248	...
F_λ(6225 Å)	6150–6300	...
Hβ	4750–4930	4700–4750, 5080–5120
Hα	6300–6790	6100–6300, 6800–6940
ESO 141−G55		
F_λ(4200 Å)	4180–4220	...
F_λ(5110 Å)	5090–5130	...
F_λ(6240 Å)	6200–6280	...
Hγ	4280–4425	4180–4220, 4425–4465
He II λ4686[a]	4465–4725	4425–4465, 4725–4770
Hβ	4770–4745	4725–4770, 5090–5130
He I λ5876	5870–5980	5700–5780, 6000–6080
Hα	6380–6800	6200–6280, 6800–6860
AKN 120		
F_λ(4200 Å)	4180–4220	...
F_λ(5630 Å)	5580–5680	...
Hγ	4265–4420	4180–4220, 4420–4460
Hβ	4770–4930	4730–4770, 5080–5120
Hα	6350–6700	6200–6280, 6740–6820
Fairall 9		
F_λ(4230 Å)	4200–4260	...
F_λ(5630 Å)	5480–5580	...
Hγ	4280–4420	4200–4260, 4420–4460
He II λ4686[a]	4460–4750	4420–4460, 4750–4780
Hβ	4780–4930	4750–4780, 5080–5120
Hα	6400–6700	6170–6270[b]

[a] Includes a contribution from Fe II multiplets.

[b] Continuum taken to be a constant defined by the mean value inside the window.

TABLE 5

MEASUREMENTS OF SPECTRA—IC 4329A[a]

JD (2,440,000+)	F_λ(4210 Å)	F_λ(6225 Å)	F(Hβ)	F(Hα)
8643	3.74 ± 0.20	8.82 ± 0.47	363.9 ± 20.9	3866.5 ± 113.3
8647	...	...	338.8 ± 22.7	2751.5 ± 150.4
8651	3.60 ± 0.15	8.05 ± 0.64	353.3 ± 16.7	2521.7 ± 120.2
8656	3.41 ± 0.15	8.13 ± 0.50	311.7 ± 11.0	2805.5 ± 96.9
8660	3.71 ± 0.20	8.47 ± 0.33	310.9 ± 14.9	3202.0 ± 85.3
8664	4.05 ± 0.16	9.16 ± 0.53	332.4 ± 12.1	3125.0 ± 136.2
8668	4.38 ± 0.14	9.01 ± 0.61	303.0 ± 16.5	3216.5 ± 186.2
8676	4.09 ± 0.26	8.79 ± 0.68	319.6 ± 11.6	...
8677	4.11 ± 0.30	8.44 ± 0.46	331.2 ± 23.3	3208.2 ± 116.8
8678	...	8.99 ± 0.57	306.8 ± 8.9	2965.1 ± 105.7
8704	3.91 ± 0.30	8.59 ± 0.57	288.4 ± 21.2	2904.8 ± 120.3
8712	3.51 ± 0.14	8.55 ± 0.37	309.6 ± 10.1	3004.5 ± 95.8
8720	3.54 ± 0.17	8.33 ± 0.40	308.8 ± 13.2	2915.1 ± 92.1
8724	3.55 ± 0.16	8.66 ± 0.48	324.2 ± 14.1	3071.1 ± 95.2
8728	4.54 ± 0.38	...	367.5 ± 39.4	...
8732	4.37 ± 0.16	9.24 ± 0.49	318.2 ± 30.1	3181.4 ± 130.4
8736	3.72 ± 0.19	8.54 ± 0.52	297.3 ± 15.3	2794.9 ± 79.7
8752	4.44 ± 0.17	9.75 ± 0.56	326.9 ± 16.0	3210.0 ± 125.9
8764	4.49 ± 0.17	10.13 ± 0.57	360.2 ± 14.2	3268.9 ± 102.4
8776	3.78 ± 0.14	9.25 ± 0.63	...	3352.7 ± 105.7
8794	3.41 ± 0.13	9.08 ± 0.58	332.7 ± 13.9	3396.5 ± 112.0
8808	3.72 ± 0.18	9.77 ± 0.50	384.0 ± 18.9	3473.6 ± 121.0
8822	3.72 ± 0.22	9.44 ± 0.41	366.8 ± 17.4	3422.3 ± 92.7
8824	3.64 ± 0.15	9.09 ± 0.48	347.5 ± 24.6	3312.0 ± 103.3
8826	3.99 ± 0.19	10.05 ± 0.60	370.6 ± 27.5	3640.8 ± 132.6
8830	3.83 ± 0.13	9.43 ± 0.38	346.8 ± 12.8	3268.2 ± 75.9
8832	3.72 ± 0.20	10.06 ± 0.62	340.3 ± 18.2	3420.3 ± 140.9

[a] Continuum fluxes in units of 10^{-15} ergs cm^{-2} s^{-1} Å^{-1} and line fluxes in units of 10^{-15} ergs cm^{-2} s^{-1}.

galaxy (Salamanca et al. 1994; Paper I). By using the continuum energy distribution of the stellar population's spectrum, we can obtain an estimate of the contribution at other wavelengths.

For the objects studied here, we are however faced with the problem of identifying the correct template for the host galaxy. In IC 4329A, the morphological classification is uncertain as a result of the high inclination of the galaxy, while in Fairall 9, this uncertainty is a consequence of the brightness of the nucleus. If we suppose that the host galaxy of IC 4329A can be represented as a late-type lenticular (SA0+:; de Vaucouleurs et al. 1991) and use the equivalent widths of the appropriate E/S0 template published by Bica (1988), the contribution from the underlying stellar population is ~20% at 3933 Å (the Ca II K λ3933 absorption line; W_{AGN} = 3.0 Å), and ~35% at 5175 Å (the Mg I + Mg h λ5175 band; W_{AGN} = 2.5 Å). For Fairall 9, Véron-Cetty, Woltjer, & Roy (1991) found that the colors and luminosity profile of the underlying galaxy are compatible with those of a luminous giant elliptical, and a comparison with the E1 template indicates a contribution of ~10% from the stellar population to the nuclear continuum at 3933 Å in the mean spectrum corresponding to the JD 2,448,808–2,448,834 low state.

Since the actual spectral energy distribution of the host galaxy of IC 4329A is affected by the strong internal reddening and we do not know either the value of the

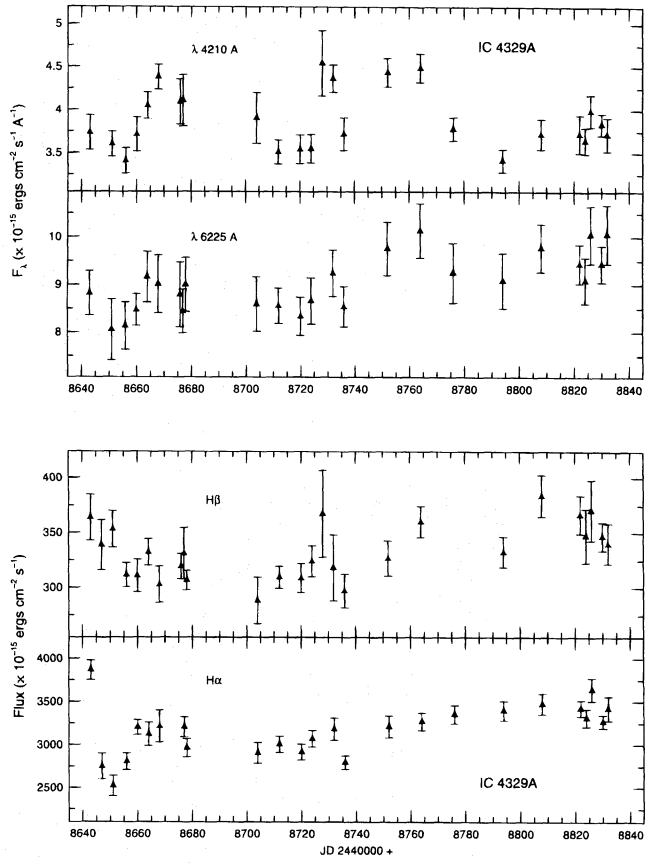

FIG. 3.—IC 4329A light curves. *Top*, 4210 and 6225 Å continua; *bottom*, Hβ and Hα.

TABLE 6

MEASUREMENTS OF SPECTRA—ESO 141−G55[a]

JD (2,440,000+)	F_λ(4200 Å)	F_λ(5510 Å)	F_λ(6240 Å)	F(Hγ)	F(He II λ4686)[b]	F(Hβ)	F(He I λ5876)	F(Hα)
8704	10.71 ± 0.17	7.68 ± 0.17	5.51 ± 0.25	217.2 ± 15.7	156.1 ± 32.9	503.4 ± 18.0	127.0 ± 22.6	1690.9 ± 67.1
8712	9.26 ± 0.13	6.50 ± 0.14	5.01 ± 0.30	182.0 ± 9.2	180.6 ± 19.9	500.7 ± 14.4	104.0 ± 20.6	1707.6 ± 62.1
8716	8.50 ± 0.17	6.44 ± 0.15	4.93 ± 0.22	209.3 ± 9.5	147.9 ± 19.0	508.3 ± 15.4	119.8 ± 22.8	1860.0 ± 58.4
8720	8.92 ± 0.31	6.65 ± 0.14	5.05 ± 0.30	243.1 ± 15.0	171.7 ± 11.7	522.5 ± 9.7	86.8 ± 17.7	1669.3 ± 87.7
8724	7.96 ± 0.13	6.35 ± 0.10	4.92 ± 0.22	224.6 ± 13.9	154.7 ± 24.8	502.2 ± 10.2	113.5 ± 16.1	1759.7 ± 54.3
8728	7.38 ± 0.34	6.03 ± 0.65	4.49 ± 0.65	197.6 ± 18.3	115.1 ± 29.1	473.4 ± 26.4	136.4 ± 50.2	1488.0 ± 130.4
8732	7.17 ± 0.18	5.71 ± 0.17	4.57 ± 0.40	171.4 ± 12.9	147.0 ± 19.0	452.6 ± 12.5	97.6 ± 27.7	1524.6 ± 89.7
8736	8.12 ± 0.17	5.93 ± 0.15	4.51 ± 0.27	201.5 ± 13.5	195.1 ± 22.9	518.1 ± 12.9	73.6 ± 19.0	1578.9 ± 58.5
8752	7.28 ± 0.16	5.57 ± 0.11	4.33 ± 0.35	178.4 ± 8.9	133.7 ± 14.4	484.1 ± 11.0	68.7 ± 23.5	1737.2 ± 65.8
8764	6.96 ± 0.36	5.31 ± 0.13	4.38 ± 0.26	167.3 ± 22.2	119.2 ± 31.7	444.6 ± 16.2	56.1 ± 29.1	1605.1 ± 74.0
8772	7.52 ± 0.38	5.75 ± 0.15	4.42 ± 0.31	223.7 ± 21.4	148.8 ± 29.2	504.2 ± 16.9	115.4 ± 25.7	1760.7 ± 64.1
8776	7.46 ± 0.22	5.96 ± 0.17	4.64 ± 0.23	186.8 ± 14.7	146.5 ± 22.7	465.4 ± 14.8	99.6 ± 19.0	1716.2 ± 48.0
8783	7.18 ± 0.17	5.82 ± 0.18	4.90 ± 0.22	184.9 ± 10.7	128.8 ± 13.5	451.3 ± 11.6	82.1 ± 24.0	1878.0 ± 55.0
8794	8.97 ± 0.25	7.27 ± 0.22	...	194.1 ± 16.7	101.7 ± 33.0	458.8 ± 22.4	114.2 ± 32.1	...
8802	8.07 ± 0.22	6.01 ± 0.14	4.61 ± 0.29	163.0 ± 12.9	136.2 ± 21.5	422.0 ± 14.5	78.3 ± 20.2	1704.5 ± 60.7
8804	8.06 ± 0.26	5.95 ± 0.26	...	191.7 ± 12.9	125.0 ± 13.9	402.6 ± 16.6	81.0 ± 25.3	...
8808	7.80 ± 0.15	6.00 ± 0.17	4.50 ± 0.29	166.1 ± 10.9	128.9 ± 23.2	418.2 ± 16.3	68.1 ± 24.6	1699.0 ± 57.6
8810	8.07 ± 0.22	6.12 ± 0.22	4.70 ± 0.30	165.4 ± 13.2	134.2 ± 25.0	404.7 ± 19.9	69.9 ± 25.5	1720.5 ± 64.2
8812	6.85 ± 0.34	5.00 ± 0.33	3.98 ± 0.34	144.4 ± 17.9	112.8 ± 27.7	395.2 ± 26.2	44.2 ± 23.5	1601.3 ± 59.0
8822	7.54 ± 0.37	5.40 ± 0.20	4.22 ± 0.33	123.7 ± 17.8	138.7 ± 17.3	368.2 ± 14.9	76.6 ± 18.2	1671.2 ± 69.4
8824	7.65 ± 0.19	5.84 ± 0.11	4.56 ± 0.34	144.4 ± 12.3	114.8 ± 23.6	376.9 ± 14.3	73.7 ± 19.6	1748.3 ± 73.0
8826	7.62 ± 0.29	6.23 ± 0.23	...	172.3 ± 18.8	110.7 ± 34.6	402.5 ± 23.2	...	...
8830	7.60 ± 0.18	6.10 ± 0.10	4.74 ± 0.28	177.1 ± 9.9	122.5 ± 12.7	449.1 ± 8.7	100.2 ± 18.9	1973.6 ± 58.4
8832	7.30 ± 0.29	5.59 ± 0.12	4.62 ± 0.21	147.5 ± 13.5	109.3 ± 12.5	446.0 ± 9.9	79.8 ± 29.6	1902.2 ± 58.5

[a] Continuum fluxes in units of 10^{-15} ergs cm^{-2} s^{-1} Å^{-1} and line fluxes in units of 10^{-15} ergs cm^{-2} s^{-1}.
[b] Plus Fe II multiplets.

intrinsic color excess or whether a Galactic reddening law is actually valid in this galaxy (Brindle et al. 1990; Winkler et al. 1992), we decided against applying any kind of correction for the contamination of the stellar population in the light curves derived for this object. For Fairall 9, the underlying galaxy's contribution is small enough, and our observations too sparsely sampled (so no time-series analysis is possible), for this correction to be necessary.

As we are interested only in the variability of the continuum and emission lines, we opted to measure the features of interest in the simplest way. All emission lines were measured by interpolating a linear continuum, defined by two windows on each side of the line, underneath the broad feature and integrating all flux above this continuum in a fixed interval. The errors were obtained by multiplying the rms of the continuum flux neighboring each line by the width of the line's integration interval. The continuum errors are just the rms flux inside the respective bands. Table 4 shows the continuum windows and line integration intervals for all objects. The Hα line in Fairall 9 is located near the border of the spectrum, so it is impossible to define a red window for the continuum fitting; we assumed that this could be represented by the mean value inside the window at the blue side of the line. The flux measurements

TABLE 7

MEASUREMENTS OF SPECTRA—ARAKELIAN 120[a]

JD (2,440,000+)	F_λ(4200 Å)	F_λ(5630 Å)	F(Hγ)	F(Hβ)	F(Hα)
8619	...	6.02 ± 0.34	119.6 ± 32.0	522.2 ± 22.8	1712.8 ± 136.2
8623	10.38 ± 0.14	6.91 ± 0.15	176.5 ± 11.1	585.0 ± 9.7	2185.9 ± 59.0
8627	8.90 ± 0.18	5.79 ± 0.24	153.7 ± 11.1	471.1 ± 15.4	1819.5 ± 42.4
8631	9.28 ± 0.21	6.22 ± 0.20	154.3 ± 13.6	513.6 ± 11.9	2116.5 ± 60.3
8635	9.96 ± 0.23	6.55 ± 0.22	165.3 ± 15.4	536.1 ± 14.9	2128.9 ± 62.4
8643	10.34 ± 0.22	7.01 ± 0.23	183.4 ± 16.8	614.2 ± 16.2	2380.7 ± 46.1
8647	10.39 ± 0.27	6.77 ± 0.20	193.2 ± 16.4	659.6 ± 15.5	2172.0 ± 50.4
8651	9.94 ± 0.28	6.66 ± 0.21	197.7 ± 19.2	625.7 ± 16.8	1984.1 ± 61.9
8656	10.83 ± 0.24	7.28 ± 0.26	211.1 ± 17.9	656.8 ± 9.1	2154.3 ± 71.8
8660	9.85 ± 0.25	6.96 ± 0.22	211.1 ± 25.4	626.7 ± 12.9	2023.8 ± 50.2
8664	9.28 ± 0.22	6.13 ± 0.15	173.2 ± 15.7	550.6 ± 13.6	1673.6 ± 37.8
8668	10.80 ± 0.30	7.16 ± 0.24	174.6 ± 10.9	643.3 ± 29.8	1967.0 ± 59.1
8672	9.44 ± 0.14	6.32 ± 0.26	185.1 ± 16.0	573.4 ± 18.3	2080.0 ± 75.9
8676	10.37 ± 0.33	6.86 ± 0.30	242.9 ± 19.4	647.5 ± 16.4	2567.5 ± 54.1
8678	9.90 ± 0.27	7.02 ± 0.22	210.8 ± 18.8	649.1 ± 18.4	2654.9 ± 85.5
8830	9.97 ± 0.09	7.08 ± 0.26	212.8 ± 8.5	658.4 ± 21.7	2564.9 ± 56.1
8832	9.56 ± 0.34	7.17 ± 0.19	209.7 ± 17.8	633.4 ± 13.9	2726.8 ± 70.4
8834	10.45 ± 0.31	6.96 ± 0.23	235.6 ± 23.9	667.1 ± 17.1	2341.2 ± 88.6

[a] Continuum fluxes in units of 10^{-15} ergs cm^{-2} s^{-1} Å^{-1} and line fluxes in units of 10^{-15} ergs cm^{-2} s^{-1}.

TABLE 8

MEASUREMENTS OF SPECTRA—FAIRALL 9[a]

JD (2,440,000+)	F_λ(4230 Å)	F_λ(5630 Å)	F(Hγ)	F(He II λ4686)[b]	F(Hβ)	F(Hα)
8607.....	6.87 ± 0.26	4.93 ± 0.28	96.2 ± 19.3	133.8 ± 35.8	307.5 ± 16.9	1362.2 ± 72.1
8619.....	6.87 ± 0.17	4.30 ± 0.19	135.7 ± 12.0	137.2 ± 22.9	301.9 ± 12.4	...
8623.....	5.75 ± 0.11	4.56 ± 0.19	95.7 ± 8.2	127.5 ± 16.9	311.1 ± 6.9	1007.2 ± 20.9
8627.....	5.89 ± 0.11	4.68 ± 0.21	114.6 ± 5.9	152.1 ± 10.0	317.4 ± 7.2	1108.2 ± 37.7
8631.....	6.37 ± 0.18	4.86 ± 0.17	119.8 ± 9.2	170.1 ± 11.6	343.0 ± 5.5	1131.6 ± 18.7
8635.....	6.05 ± 0.20	4.75 ± 0.12	110.3 ± 12.3	137.0 ± 17.7	326.5 ± 7.1	1106.3 ± 40.6
8639.....	6.01 ± 0.14	4.39 ± 0.21	100.6 ± 11.5	106.3 ± 20.0	294.2 ± 6.9	...
8808.....	3.85 ± 0.14	3.55 ± 0.20	108.0 ± 7.6	90.7 ± 17.5	240.1 ± 8.8	1132.0 ± 28.2
8822.....	4.21 ± 0.20	4.03 ± 0.27	108.3 ± 15.2	65.4 ± 34.8	...	...
8824.....	3.56 ± 0.13	3.60 ± 0.26	102.2 ± 8.0	70.8 ± 19.0	235.0 ± 9.6	1112.4 ± 49.2
8830.....	3.60 ± 0.13	3.31 ± 0.16	92.5 ± 7.3	77.8 ± 10.5	243.9 ± 6.1	1062.5 ± 37.7
8832.....	3.80 ± 0.10	3.53 ± 0.22	93.0 ± 8.4	79.8 ± 19.3	241.4 ± 9.5	1185.3 ± 25.1
8834.....	3.96 ± 0.24	3.44 ± 0.20	93.6 ± 14.6	95.2 ± 21.1	253.0 ± 8.0	1148.7 ± 39.4

[a] Continuum fluxes in units of 10^{-15} ergs cm^{-2} s^{-1} Å^{-1} and line fluxes in units of 10^{-15} ergs cm^{-2} s^{-1}.
[b] Plus Fe II multiplets.

are listed in Tables 5–8, and the light curves for the continua and emission lines measured in the IC 4329A and ESO 141−G55 spectra are shown in Figures 3, 4, and 5. The Hγ line in all objects is contaminated by the [O III] λ 4363 emission line, and He II λ4686 is contaminated by Fe II multiplets. We have excluded from these tables the epochs in which the low S/N of the spectra (due to poor weather or full moon) or suspected calibration problems resulted in flux errors greater than 20%, except for the low-contrast features (He II λ4686 and He I λ5876), where we excluded only the measurements in which obvious problems of calibration could be detected.

4. VARIABILITY ANALYSIS

4.1. *Variability Amplitude*

The general characteristics of the database for each object studied here are summarized in Table 9. The parameters R_{max} and F_{var} are the ratios of the maximum to minimum flux observed and of the rms fluctuation amplitude to the mean flux (corrected for the effect of the measurement errors), respectively (Clavel et al. 1991). In column (8), we present the reduced χ^2 for variability with respect to the mean and, in column (9), the probability of obtaining that result under the hypothesis of constant flux (no real variability). It can be seen that this hypothesis is strongly rejected in most cases [P(null) < 10^{-4}], with the exception of He I λ5876 in ESO 141−G55 and most of the features inside each group of observations for Fairall 9. While our data indicate little variability in the continuum and emission lines of Fairall 9 on timescales of a few days to 1

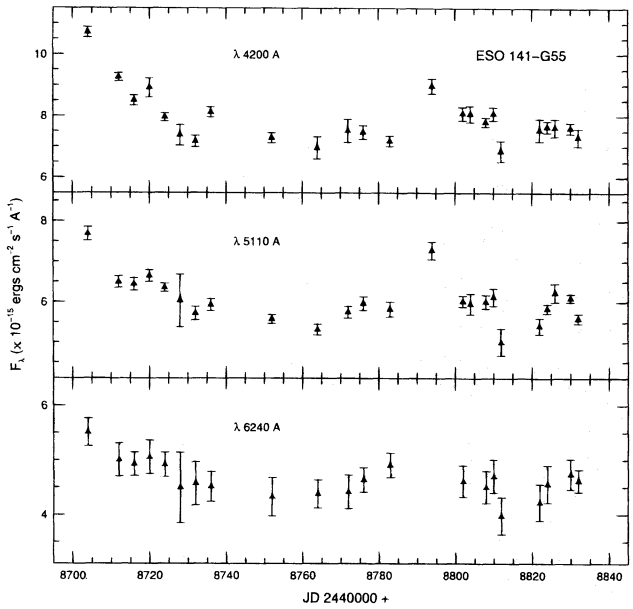

FIG. 4.—ESO 141−G55 continuum light curves: 4200, 5110, and 6240 Å continua (*top to bottom*).

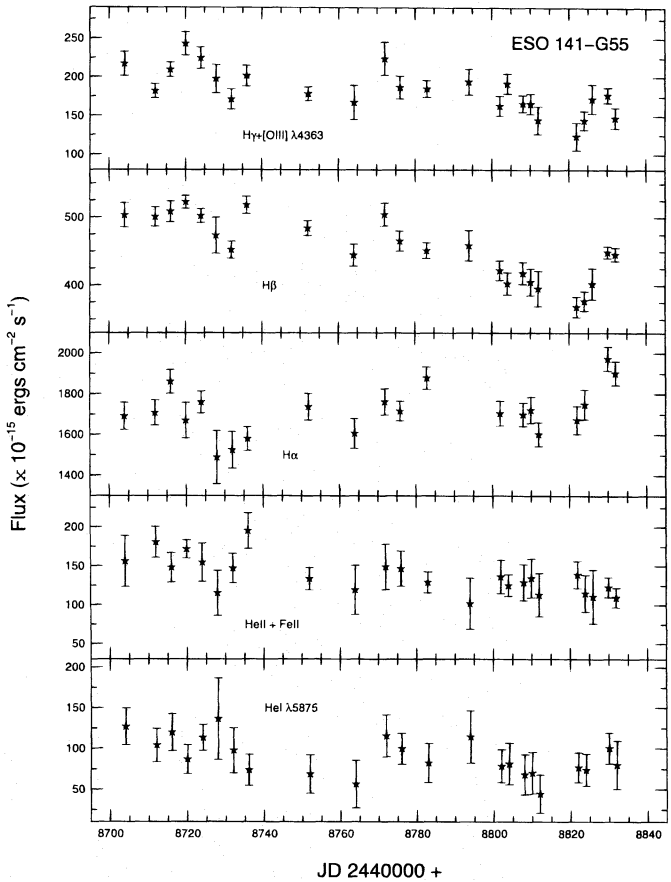

FIG. 5.—ESO 141−G55 broad emission line light curves: Hγ + [O III] λ4363, Hβ, Hα, He II λ4686 + Fe II, and He I λ5875 (*top to bottom*).

TABLE 9

VARIABILITY PARAMETERS AND SAMPLING CHARACTERISTICS

Feature (1)	Number of Epochs (2)	Sampling Interval (days) Average (3)	Sampling Interval (days) Median (4)	Mean Flux[a] (5)	F_{var} (6)	R_{max} (7)	$\chi^{2\,b}_{\nu}$ (8)	P(null)[c] (9)
IC 4329A								
F_λ(4210 Å)	25	7.88	4	3.88	0.08	1.33	4.18	$<10^{-4}$
F_λ(6225 Å)	25	7.88	4	9.03	0.05	1.26	1.38	0.9
Hβ	26	7.56	4	333.1	0.08	1.33	2.46	$<10^{-4}$
Hα	25	7.88	4	3172.0	0.09	1.53	7.20	$<10^{-4}$
ESO 141−G55								
F_λ(4200 Å)	24	5.57	4	7.92	0.10	1.56	22.34	$<10^{-4}$
F_λ(5110 Å)	24	5.57	4	6.05	0.09	1.54	11.51	$<10^{-4}$
F_λ(6240 Å)	21	6.40	4	4.65	0.07	1.38	1.40	0.9
Hγ.....	24	5.57	4	182.4	0.16	1.97	3.74	$<10^{-4}$
He II λ4686[d].....	24	5.33	4	138.8	0.18	1.92	1.51	0.9
Hβ	24	5.57	4	453.1	0.10	1.42	10.69	$<10^{-4}$
He I λ5876	23	5.82	4	89.8	0.26	3.09	0.91	>0.5
Hα	21	6.40	4	1714.1	0.07	1.33	3.31	$<10^{-4}$
AKN 120—JD 2,448,629 to 2,448,678								
F_λ(4200 Å)	14	4.23	4	9.98	0.05	1.22	8.27	$<10^{-4}$
F_λ(5630 Å)	15	4.21	4	6.65	0.06	1.26	4.06	$<10^{-4}$
Hγ.....	15	4.21	4	183.5	0.16	2.03	2.47	0.995
Hβ	15	4.21	4	591.7	0.10	1.40	17.55	$<10^{-4}$
Hα	15	4.21	4	2108.1	0.13	1.59	25.08	$<10^{-4}$
AKN 120—All Data								
F_λ(4200 Å)	17	...	4	9.98	0.08	1.34	6.97	$<10^{-4}$
F_λ(5630 Å)	18	...	4	6.72	0.06	1.26	3.99	$<10^{-4}$
Hγ.....	18	...	4	189.5	0.16	2.03	3.09	$<10^{-4}$
Hβ	18	...	4	601.9	0.10	1.42	16.30	$<10^{-4}$
Hα	18	...	4	2180.8	0.14	1.63	30.10	$<10^{-4}$
Fairall 9—JD 2,448,607 to 2,448,639								
F_λ(4230 Å)	7	...	...	6.26	0.06	1.19	9.09	$<10^{-4}$
F_λ(5630 Å)	7	...	...	4.64	0.03	1.15	1.39	0.75
Hγ.....	7	...	...	110.4	0.13	1.42	1.75	0.75
He II λ4686[d].....	7	...	...	137.8	0.14	1.60	2.12	0.9
Hβ	7	...	...	314.5	0.05	1.17	6.69	$<10^{-4}$
Hα	5	...	...	1143.1	0.12	1.35	13.38	$<10^{-4}$
Fairall 9—JD 2,448,808 to 2,448,834								
F_λ(4230 Å)	6	...	...	3.83	0.04	1.18	2.37	0.9
F_λ(5630 Å)	6	...	...	3.58	0.04	1.22	1.27	0.7
Hγ.....	6	...	...	99.6	0.08	1.17	0.68	>0.5
He II λ4686[d].....	6	...	...	80.0	0.14	1.46	0.27	>0.5
Hβ	5	...	...	242.7	0.03	1.08	0.61	>0.5
Hα	5	...	...	1128.2	0.04	1.12	2.15	0.9
Fairall 9—All Data								
F_λ(4230 Å)	13	...	...	5.14	0.24	1.93	76.80	$<10^{-4}$
F_λ(5630 Å)	13	...	...	4.15	0.13	1.48	10.64	$<10^{-4}$
Hγ.....	13	...	...	105.4	0.12	1.47	1.63	0.9
He II λ4686[d].....	13	...	...	111.1	0.31	2.60	5.70	$<10^{-4}$
Hβ	12	...	...	284.6	0.14	1.46	29.38	$<10^{-4}$
Hα	10	...	...	1135.6	0.08	1.35	6.30	$<10^{-4}$

[a] In units of 10^{-15} ergs cm^{-2} s^{-1} Å^{-1} for the continua and 10^{-15} ergs cm^{-2} s^{-1} for the lines.
[b] Reduced χ^2 for variability about the mean. Degrees of freedom are the number of epochs $N-1$ for each feature.
[c] Probability of obtaining the calculated value of χ^2_ν if no real variability is present.
[d] Plus Fe II multiplets.

month, the analysis of the complete set of observations shows that this object can vary by a factor of ~2 in both continuum and broad lines over a few months. The same is not true for AKN 120, in which the variability on short timescales (up to 50 days) does not differ too much in amplitude from the results for the complete data set, which includes observations taken 4 months apart. This behavior is consistent with the known variability history of this source (Peterson et al. 1989). Note also that the χ^2 test indicates that the variations observed in IC 4329A

[log $L(H\beta) \sim 41.49$; if corrected by $E(B-V) = 0.8$, this value rises to log $L(H\beta) \sim 41.96$] are of smaller amplitude than those in ESO 141−G55, a higher luminosity AGN [log $L(H\beta) \sim 42.21$]. This effect runs counter to the behavior usually observed, as in the standard-model AGN geometry the amplitude of the emission-line variations decreases with increasing luminosity as a consequence of the larger size of the BLR (Peterson 1994; Robinson 1994), and could be due to the limited temporal extension of the monitoring campaign.

4.2. *Time-Series Analysis*

Under the assumptions of the standard reverberation scenario (see Peterson 1993), the time delay between the continuum and broad emission line variations can be interpreted as an estimate of the BLR's size. For irregularly sampled data, this delay can be obtained by use of the interpolation cross-correlation (CCF) technique (White & Peterson 1994), and we can use the centroid of the distribution as a measure of the responsivity-weighted radius of the emission region (Koratkar & Gaskell 1991). In this section, we present and discuss the analysis of the light curves derived for IC 4329A and ESO 141−G55.

The first step in analyzing any time series is to determine whether the sampling is adequate. This can be accomplished by comparing the width of the autocorrelation functions (ACFs) for the series of interest with that of the sampling-window autocorrelation function (SWACF), obtained by repeatedly sampling a white-noise spectrum in the same pattern as the real observations. The FWHM of the window ACFs indicates how much artificial correlation is introduced when the observed light curves are interpolated while calculating the CCFs. We adopted the same criterion as Gaskell & Peterson (1987), considering the data to be well sampled when the true (vs. observed) FWHM of the light-curve ACF is at least 10% greater than the FWHM of the window ACF. If the ACFs are Gaussian, the observed FWHM (W_a) will be the square root of the two quantities above added in quadrature. The sampling criterion for the observed ACFs is then $W_a/W_s \gtrsim 1.35$. The comparison between the distributions for the two objects studied are shown in Figures 6 and 7. The FWHMs of the line and continuum ACFs and the ratio W_a/W_s are shown in columns (3) and (4) of Table 10, respectively.

From these data it can be seen that the light curves are slightly undersampled for IC 4329A, especially the 4210 Å continuum and Hα. Even for the cases in which the sampling was not adequate, an upper limit on the size of the emission region can be provided by the half-width at zero correlation (HWZC) of the line ACFs, as, assuming a simple spherical model, this will represent the larger coherence length of the variations, defined by the diameter of the emission region (Gaskell & Peterson 1987; Koratkar & Gaskell 1991). The results for the Hβ and Hα emission lines in IC 4329A are shown in column (5) of Table 10 and indicate an *upper* limit of ∼30 lt-days (0.03 pc) for the radius of the emission region.

For ESO 141−G55, all series satisfy the sampling criterion with the possible exception of Hα, which, although formally within the limit above, resulted in an ACF with little power for delays longer than a few days (see Fig. 7). The shape of the He II λ4686 ACF similarly indicates that the correlated errors are more important in this light curve than in the case of Hβ. Taking these facts into account, probably only the HWZC obtained from the Hβ ACF can be regarded as somewhat representative of the scale length of the variations, resulting in a *lower* limit of ∼30 lt-days for the emission region.

The results of the cross-correlation analysis are summarized in columns (6)–(8) of Table 10. Here Δt_{peak} is the lag

TABLE 10

VARIABILITY ANALYSIS

First Series (1)	Second Series (2)	FWHM (days) (3)	W_a/W_s (4)	HWZI (days) (5)	Δt_{peak} (days) (6)	Δt_{cent} (days) (7)	r_{max} (8)
IC 4329A							
F_λ(4210 Å) ACF	...	10.8	1.6	...	...	...	...
F_λ(6625 Å) ACF	...	23.9	3.5	...	...	...	...
Hβ ACF	...	15.7	2.3	60	...	...	...
Hα ACF	...	7.8	1.2	60	...	...	...
F_λ(6625 Å)	Hβ	74.4	...	...	18	15.6	0.597
F_λ(6625 Å)	Hα	76.1	...	...	23[a]	25.0[a]	0.620
SWACF[b]	...	6.8	...	...	...	...	...
ESO 141−G55							
F_λ(4200 Å) ACF	...	18.1	4.0	...	...	...	...
F_λ(5110 Å) ACF	...	13.8	3.1	...	...	...	...
F_λ(6240 Å) ACF	...	18.7	4.2	...	...	...	...
Hγ ACF	...	12.7	2.8	40	...	...	...
He II λ4686 ACF[c]	...	11.1	2.5	50	...	...	...
Hβ ACF	...	53.8	12.0	>60	...	...	...
He I λ5876 ACF	...	11.3	2.5	...	...	...	...
Hα ACF	...	9.8	2.2	...	...	...	...
F_λ(4200 Å)	F_λ(5110 Å)	18.4	...	...	0	−0.6	0.903
F_λ(4200 Å)	F_λ(6240 Å)	27.4	...	...	0	−1.6	0.811
SWACF[d]	...	4.5	...	...	...	...	...

[a] Position and centroid of the second most significant peak of the CCF.
[b] Sampling-window ACF calculated for the 6625 Å continuum light curve.
[c] Plus Fe II multiplets.
[d] Sampling-window ACF calculated for the 4200 Å continuum light curve.

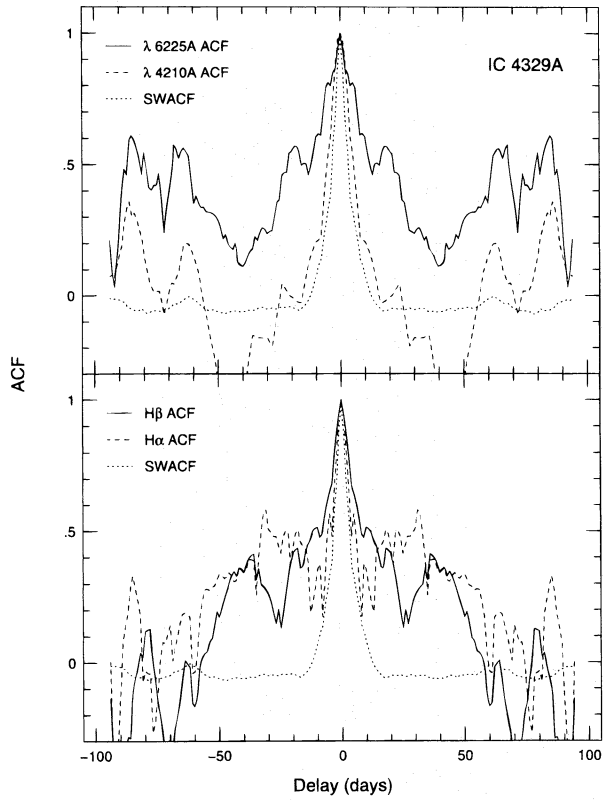

FIG. 6.—Autocorrelation functions for the continua and broad emission lines of IC 4329A. *Top*: 6225 Å (*solid line*), 4210 Å (*dashed line*), and 6225 Å sampling window (*dotted line*). *Bottom*: Hβ (*solid line*), Hα (*dashed line*), and Hβ sampling window (*dotted line*).

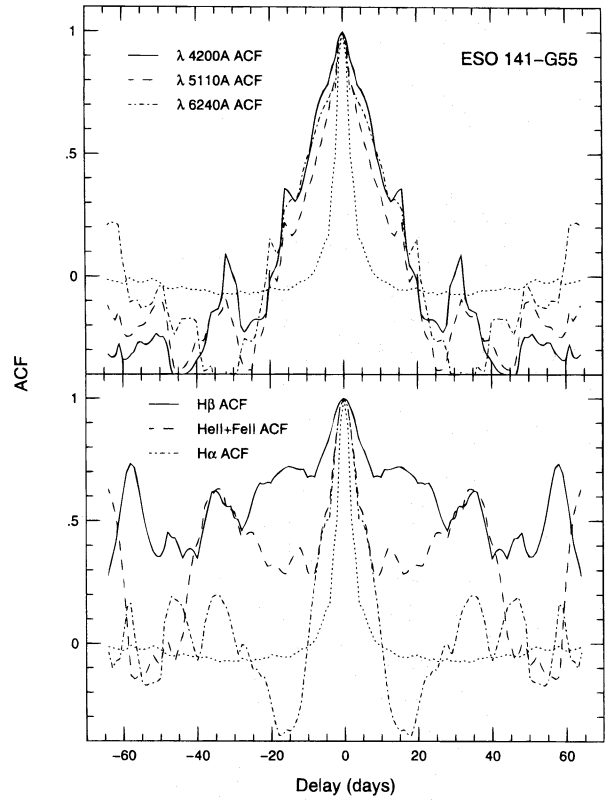

FIG. 7.—Same as Fig. 6, but for ESO 141−G55. *Top*: 4200 Å (*solid line*), 5110 Å (*dashed line*), and 6240 Å (*dot-dashed line*). *Bottom*: Hβ (*solid line*), He II λ4686 + Fe II (*dashed line*), and Hα (*dot-dashed line*). The dotted line in both panels is the 4200 Å continuum sampling-window ACF.

at which the CCF reaches its maximum value, $\Delta t_{\rm cent}$ is the position of the CCF centroid, and $r_{\rm max}$ is the peak value. The CCFs between the Hα and Hβ emission lines and the 6225 Å continuum for IC 4329A are shown in Figure 8. Both curves are contaminated by correlated errors, as evidenced by the presence of a sharp peak at zero delay, but are clearly asymmetric in the direction of positive lags, which indicates the existence of a real correlation between the lines and the continuum light curves. Besides the zero-lag peak produced by the correlated errors, the Hα CCF presents a highly significant maximum ($P \approx 99.8\%$) at $\Delta t_{\rm cent} \sim 25$ lt-days. The Hβ CCF also presents two maxima of about the same significance ($P \approx 99.8\%$), located at $\Delta t_{\rm cent} \sim 15.6$ and 51.6 lt-days. This last value would be in contradiction with the maximum size derived from the HWZC of the line ACF, so we assume that the first peak represents the actual lag between the two time series and that the second is an alias. The cross-correlation between the two continua is completely dominated by the correlated errors, as could be expected from the small width of the 4210 Å ACF.

The significance of these results can be assessed by use of Monte Carlo simulations, following the method introduced by Gaskell & Peterson (1987) and Maoz & Netzer (1989), with the modifications described in Paper I. In short, the method consists of generating a model light curve by linearly interpolating to 1 day intervals and smoothing the observed continuum, which is then convolved with the transfer function for a thin spherical shell of radius R to obtain a synthetic line light curve. The two model time series are then resampled at the same number of points as the observed ones, to preserve the number of paired observations (nights when it was possible to measure both continuum and line fluxes from the same spectrum) and the distribution of intervals between the emission-line observations, and Gaussian-distributed random noise comparable to the observational errors is added to each point. The data sets are then cross-correlated to determine the location of the centroid of the CCF, setting a minimum confidence level based on the peak value of the CCF, ρ, as a condition for a given trial to be taken as successful and the result registered. The light curves are then resampled and the process repeated a large number of times for a given R. The result is a probability distribution for the possible values of the CCF centroid that can be obtained from the observed light curves, given the amplitude of the variations, the observational sampling and errors, and the assumed size and geometry of the BLR. For reasonably well defined lags, the width of the probability distribution can be regarded as an estimate of the error in the observed delay, while for less well sampled series, we can use the method to explore the probability space around the observed result allowed by the observational data.

The simulations were run for a series of model BLRs with radii between 1 and 60 lt-days, with the confidence level set to 99.8% ($\rho = 0.544$ and 0.534 for $N = 25$ and 26 points, respectively). For both series, if the BLR's radius R is 5 lt-days, the probability that a single set of observations will produce a 99.8% significant lag of greater than 30 days is $\sim$0.18. On the other hand, if $R = 40$ lt-days, a single experiment will produce a significant lag that is smaller than 10 days $\sim$10% of the time. The results are shown in Figure 9, in which the curves present, as a function of the size of the model BLR, (*a*) the probability that the samples will

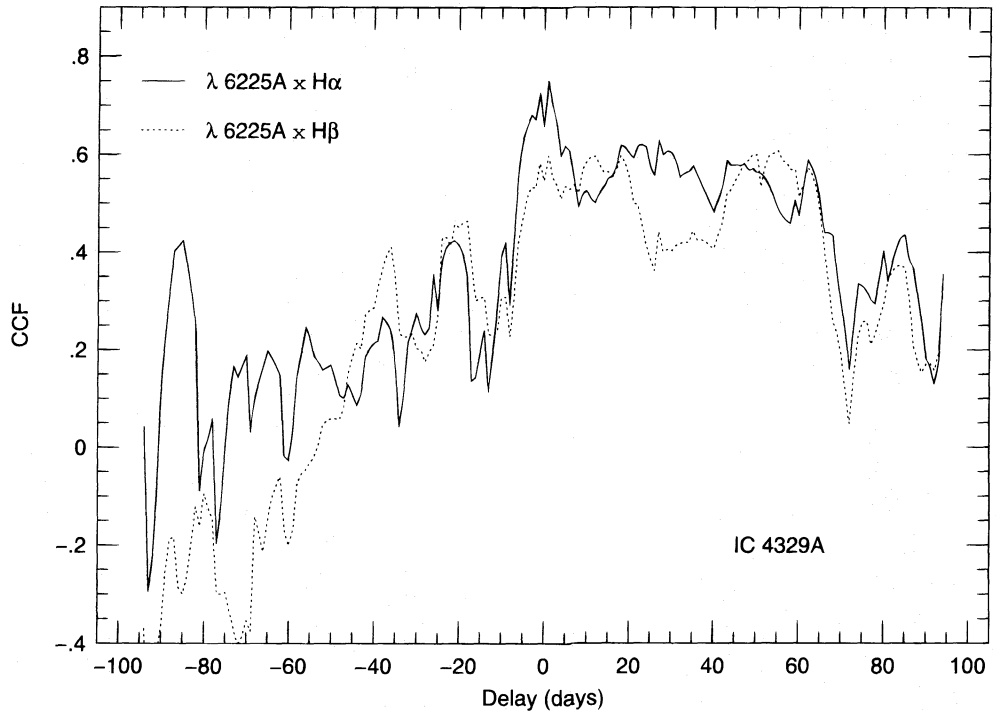

FIG. 8.—Cross-correlation between the 6225 Å continuum and the Hα (*solid line*) and Hβ (*dotted line*) emission lines of IC 4329A

produce a delay smaller than 30 days, consistent with the upper limit set by the line ACFs, and (*b*) a result within the interval 10 days $< \tau_{LT} <$ 30 days, so as to include the CCF lags obtained for both lines.

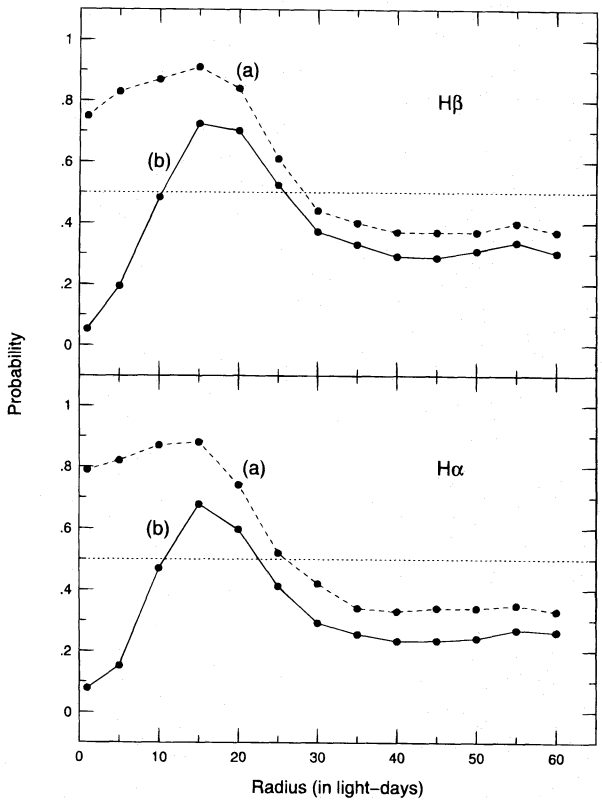

FIG. 9.—Results of the Monte Carlo simulations for Hβ (*top*) and Hα (*bottom*) of IC 4329A, as a function of the model BLR radius. The curves labeled "(a)" represent the probability that the observed samples will yield a delay smaller than 30 days, while the curves labeled "(b)" represent the probability of obtaining a CCF result within the interval 10 days $< \tau_{LT} <$ 30 days. The dotted line is the 50% probability level.

Curve *a* demonstrates that, if the BLR is indeed small ($R \lesssim 25$ lt-days), 80% or more of the samples will lead to the observed result. It is worth noting that, even when the BLR's radius is 40 lt-days or more, there is a ~40% probability that the cross-correlations will yield a size determination smaller than 30 lt-days. This effect is due to the limited temporal coverage of the monitoring and the low amplitude of the observed variations. From curve *b*, we can see that the range of model BLR sizes that will result in a cross-correlation lag in the range 10–30 days at least at the 50% level is 11 lt-days $\lesssim R \lesssim$ 25 lt-days. This interval represents the most likely lag between the continuum and line variations, but other values within the range 0–60 lt-days cannot be ruled out with a high level of confidence based on the present data.

Figure 10 shows the 5110 and 6240 Å continua and the He II λ4686 and Hβ emission lines versus the 4200 Å continuum CCFs for ESO 141−G55. The continuum CCFs peak at zero delay, indicating that the optical continuum in this object varies in phase within the resolution of our data (~4 days). As the amplitude of the variations increases for shorter wavelengths, this implies that the spectrum is bluer when the source is brighter, as has been observed for several other AGNs (Edelson, Krolik, & Pike 1990). The clearest correlation between the emission lines and the continuum occurs at zero lag and is of low significance (95% confidence level), being associated with the correlated errors, as the shape of the CCF does not differ significantly from that of the ACF. The CCFs rise at large delays, but the temporal extent of our campaign was not long enough to tell whether this is due to the presence of a real peak on the cross-correlation function located at a lag greater than 60 days.

4.3. *Profile Variability*

Although the large gaps in the temporal coverage preclude a similar time-series analysis for the AKN 120 and Fairall 9 data, it is interesting to point out the strong flux

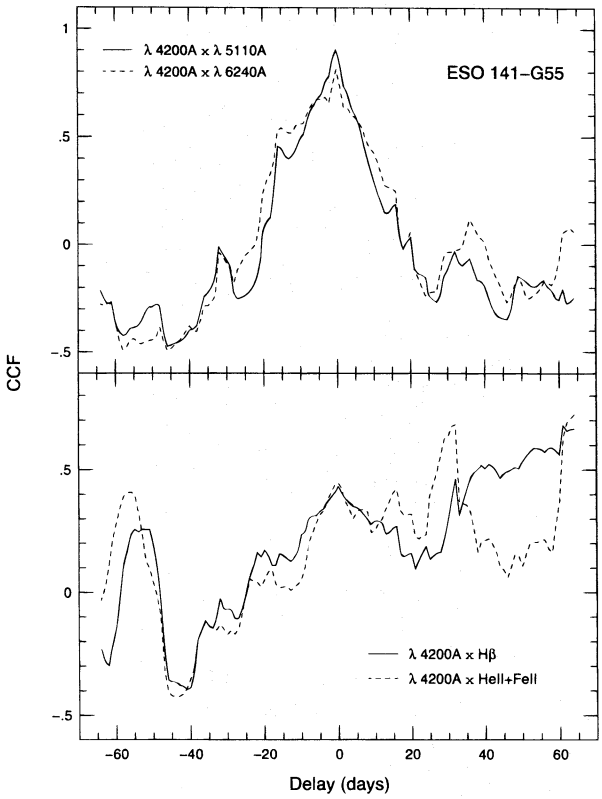

FIG. 10.—Cross-correlation between the 4200 Å continuum of ESO 141−G55 and the 5110 Å (*solid line*) and 6240 Å (*dashed line*) continua (*top*) and the Hβ (*solid line*) and He II λ4686+Fe II (*dashed line*) emission lines (*bottom*).

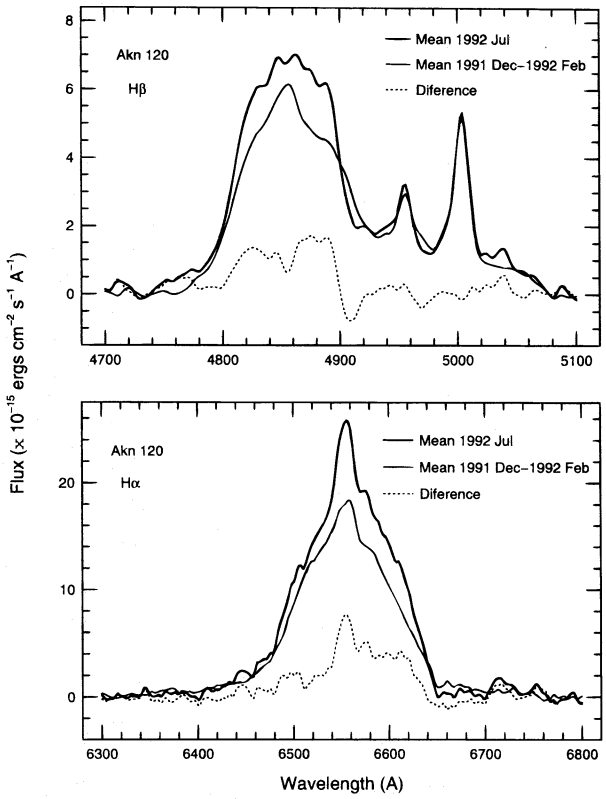

FIG. 12.—Broad-line profile variation between the mean spectra of AKN 120. *Top*, the Hβ spectral region; *bottom*, the Hα region. A linear continuum was subtracted from both spectra to highlight the profile variations (see § 4.3 for details).

and profile variations experienced by the main Balmer lines in these two objects during the period covered by our observations.

In Figure 11 are shown the mean spectra of the two sets of observations of AKN 120 (1991 December–1992 February, excluding JD 2,448,619 and 2,448,668, and 1992 July), as well as the difference between them. Note the strong flux variation in the Balmer lines (by factors of 1.4–2.0; see

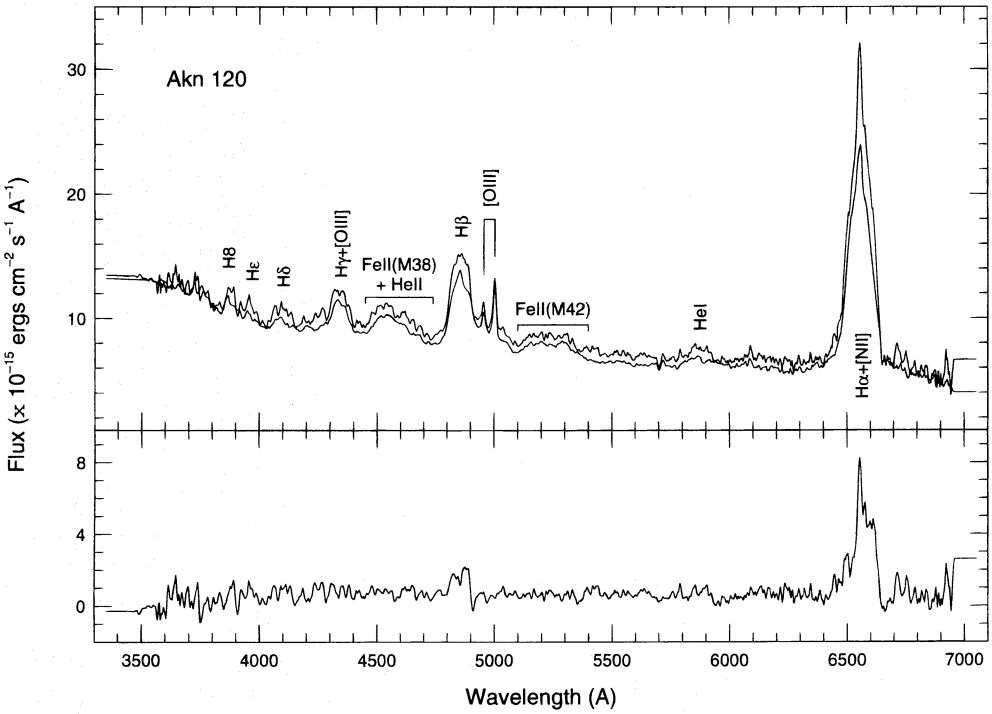

FIG. 11.—*Top*: AKN 120 mean spectra for 1991 December–1992 February (*lower spectrum*) and 1992 July (*upper spectrum*). *Bottom*: The difference spectrum.

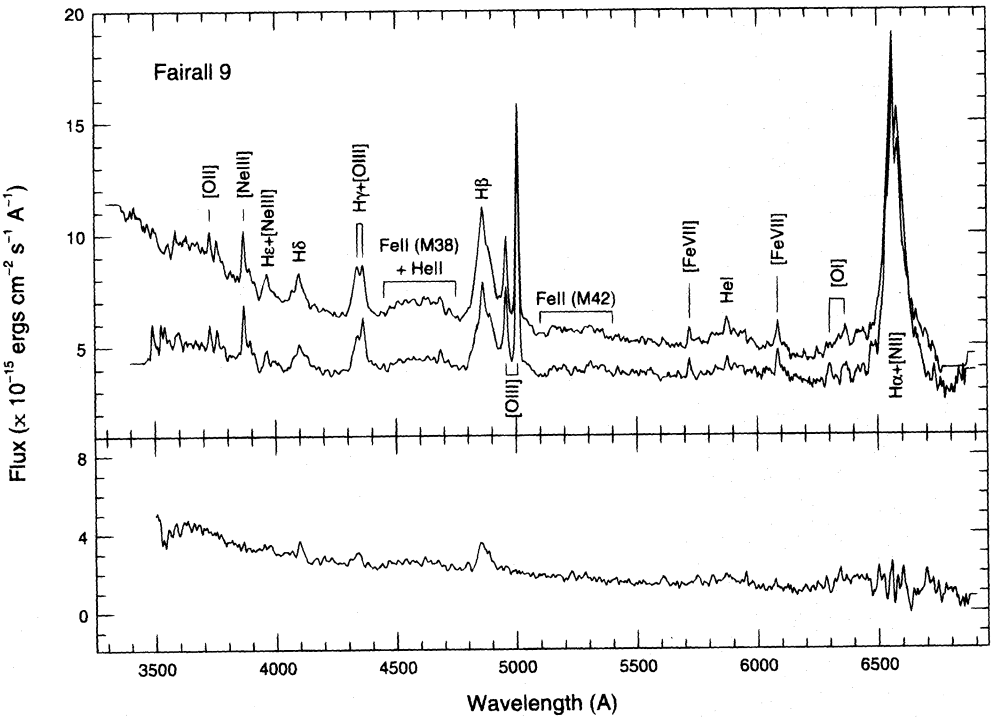

FIG. 13.—Same as Fig. 11, but for Fairall 9

Table 9) and the almost complete disappearance of the Fe II multiplets in the difference spectrum. To bring out the line-profile variations more clearly, we subtracted a local linear continuum, defined by the same windows presented in Table 4, interpolated under the line of interest in the two mean spectra. The results are shown in Figure 12 for Hα and Hβ. Note the sharp cut at the red wing in both lines and the very good subtraction of the [O III] λ5007 lines in the Hβ region.

Figure 13 shows the two mean spectra of Fairall 9 (1991 December–1992 January, excluding JD 2,448,619 and 2,448,639, and 1992 July, excluding JD 2,448,818 and 2,448,822), and their difference. In contrast to the case of AKN 120, both line and continuum levels were significantly lower in the second set of observations. As has been detected previously in other objects (Antonucci & Cohen 1983; Robinson 1994), there is a trend for the higher order Balmer lines to present larger amplitudes of variability. The decrease in flux between the two sets of observations corresponds to variations of 37%, 29%, 25%, 26%, and 8% in the fluxes of Hε, Hδ, Hγ, Hβ, and Hα, respectively, in the December/January spectrum. Finally, in Figure 14, we

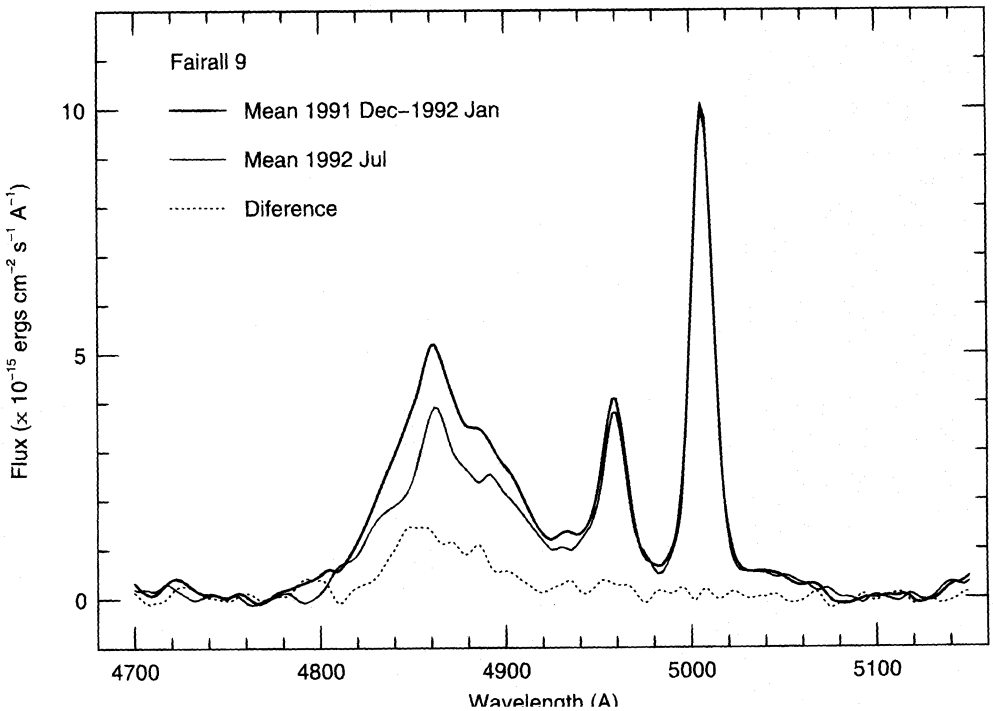

present the Hβ region in the two mean spectra, with a local continuum subtracted using the same procedure as for AKN 120, to show the profile variability. The line profile is smoother in this object than in AKN 120, and most of the changes were due to a decrease in the blue wing of the line.

5. CONCLUSIONS

We have presented the data from a campaign of optical spectroscopic monitoring of four southern active galaxies, IC 4329A, ESO 141−G55, AKN 120, and Fairall 9. Continuum and broad-line variability were detected in all objects, and the results of the campaign can be summarized as follows:

1. The mean contribution of the underlying stellar population to the nuclear spectrum of IC 4329A during the monitoring was ∼20% of the nuclear continuum at 3933 Å and 35% at 5175 Å. Assuming that the underlying galaxy of Fairall 9 is a giant elliptical, we conclude that the stellar population contributed with 10% or less of the nuclear continuum at 3933 Å when the source was in a "low" state of activity. For the two other objects studied, ESO 141−G55 and AKN 120, the stellar signatures were at the noise level, diluted by the AGN emission.

2. From the autocorrelation functions of the broad emission lines, we obtain an *upper* limit of ∼30 lt-days for the size of the emission region of IC 4329A. The cross-correlation analysis between the continuum and the emission-line light curves of IC 4329A indicates that the most likely lag between the 6225 Å continuum variations and the response of Hα and Hβ lines is in the range 15–25 days. For ESO 141−G55, the continuum from ∼4000 to ∼6500 Å was found to vary in phase within the time resolution of our data.

3. Strong broad-line flux and profile variations were observed in both AKN 120 and Fairall 9 in timescales of ∼4 months. In Fairall 9, the amplitude of the flux variations was observed to increase for the higher order Balmer lines.

C. W. acknowledges the support and hospitality of the staffs of the Cerro Tololo Inter-American Observatory and the Department of Astronomy of the Ohio State University (in particular, R. W. Pogge for making available his spectral analysis programs). This work was partly supported by NASA grant NAG5-1824 (to the Ohio State University) and the Brazilian Research Council (CNPq). This research has made use of the NASA/IPAC Extragalactic Database (NED), which is operated by the Jet Propulsion Laboratory, California Institute of Technology, under contract with NASA.

REFERENCES

Alloin, D., Boisson, C., & Pelat, D. 1988, A&A, 200, 17
Antonucci, R. R. J., & Cohen, R. D. 1983, ApJ, 271, 564
Barvainis, R. 1992, ApJ, 400, 502
Bica, E. 1988, A&A, 195, 76
Blandford, R. D., & McKee, C. F. 1982, ApJ, 255, 419
Brindle, C., Hough, J. H., Bailey, J. A., Axon, D. J., Ward, M. J., Sparks, W. B., & McLean, I. S. 1990, MNRAS, 244, 604
Burstein, D., & Heiles, C. 1984, ApJS, 54, 33
Chapman, G. N. F., Geller, M. J., & Huchra, J. P. 1985, ApJ, 297, 151
Clavel, J., et al. 1991, ApJ, 366, 64
Clavel, J., Wamsteker, W., & Glass, I. S. 1989, ApJ, 337, 236
Cooke, B. A., et al. 1978, MNRAS, 182, 489
Delvaille, J. P., Geller, M. J., & Schnopper, H. V. 1978, ApJ, 226, L69
de Vaucouleurs, G., de Vaucouleurs, A., Corwin, H. G., Buta, R. J., Paturel, G., & Fouqué, P. 1991, Third Reference Catalogue of Bright Galaxies (New York: Springer)
Dietrich, M., et al. 1994, A&A, 284, 33
———. 1993, ApJ, 408, 416
Disney, M. J. 1973, ApJ, 181, L55
Edelson, R. A., Krolik, J. H., & Pike, G. F. 1990, ApJ, 359, 86
Elvis, M., Maccacaro, T., Wilson, A. S., Ward, M. J., Penston, M. V., Fosbury, R. A. E., & Perola, G. C. 1978, MNRAS, 183, 129
Erkens, U., et al. 1995, A&A, 296, 90
Fabian, A. C., Nandra, K., Celotti, A., Rees, M. J., Grove, J. E., & Johnson, W. N. 1993, ApJ, 416, L57
Fairall, A. P. 1977, MNRAS, 180, 291
Foltz, C. B., Peterson, B. M., Capriotti, E. R., Byard, P. L., Bertram, R., & Lawrie, D. G. 1981, ApJ, 250, 508
Gaskell, C. M., & Peterson, B. M. 1987, ApJS, 65, 1
Giuricin, G., Mardirossian, F., & Mezzetti, M. 1990, ApJS, 72, 551
Hamuy, M., & Maza, J. 1987, A&AS, 68, 383
Jackson, N., et al. 1992, A&A, 262, 17
Kollatschny, W., Fricke, K. J., Schleicher, H., & Yorke, H. W. 1981, A&A, 102, L23
Koratkar, A. P., & Gaskell, C. M. 1991, ApJS, 75, 719
Korista, K. T. 1992, ApJS, 79, 285
Korista, K. T., et al. 1995, ApJS, 97, 285
Lub, J., & de Ruiter, H. R. 1992, A&A, 256, 33
Lyutyi, V. M. 1976, Astron. Tsirk., 302, 1
Marshall, N., Warwick, R. S., & Pounds, K. A. 1981, MNRAS, 194, 987
Martin, P. G., Stockman, H. S., Angel, J. P. R., Maza, J., & Beaver, E. A. 1982, ApJ, 255, 65
Marziani, P., Calvani, M., & Sulentic, J. W. 1992, ApJ, 393, 658
Maoz, D., & Netzer, H. 1989, MNRAS, 236, 21
Maoz, D., et al. 1990, ApJ, 351, 75
———. 1991, ApJ, 367, 493
Meyers, K. A., & Peterson, B. M. 1985, PASP, 97, 734
Morini, M., et al. 1986, ApJ, 307, 486
Morris, S., & Ward, M. 1988, MNRAS, 230, 639
Pastoriza, M. G. 1979, ApJ, 234, 837
Peterson, B. M. 1988, PASP, 100, 18
———. 1993, PASP, 105, 247
———. 1994, in ASP Conf. Proc. 69, Reverberation Mapping of the Broad-Line Region in Active Galactic Nuclei, ed. P. M. Gondhalekar, K. Horne, & B. M. Peterson (San Francisco: ASP), 1
Peterson, B. M., Ali, B., Horne, K., Bertram, R., Lame, N. J., Pogge, R. W., & Wagner, R. M. 1993, ApJ, 402, 469
Peterson, B. M., et al. 1992, ApJ, 392, 470
———. 1991, ApJ, 368, 119
———. 1994, ApJ, 425, 622
Peterson, B. M., & Gaskell, C. M. 1991, ApJ, 368, 152
Peterson, B. M., Korista, K. T., & Wagner, R. M. 1989, AJ, 98, 500
Peterson, B. M., Meyers, K. A., Capriotti, E. R., Foltz, C. B., Wilkes, B. J., & Miller, H. R. 1985, ApJ, 292, 164
Petre, R., Mushotzky, R. F., Krolik, J. H., & Holt, S. S. 1984, ApJ, 280, 499
Rafanelli, P. 1985, A&A, 146, 17
Reichert, G. A., et al. 1994, ApJ, 425, 582
Robinson, A. 1994, in ASP Conf. Proc. 69, Reverberation Mapping of the Broad-Line Region in Active Galactic Nuclei, ed. P. M. Gondhalekar, K. Horne, & B. M. Peterson (San Francisco: ASP), 147
Salamanca, I., et al. 1994, A&A, 282, 742
Shields, J. C., Ferland, G. J., & Peterson, B. M. 1995, ApJ, 441, 507
Stirpe, G. M. 1990, A&AS, 85, 1049
Stirpe, G. M., et al. 1994a, A&A, 285, 857
———. 1994b, ApJ, 425, 609
Stone, R. P. S., & Baldwin, J. A. 1983, MNRAS, 204, 347
Tennant, A. F., & Mushotzky, R. F. 1983, ApJ, 264, 92
Unger, S. W., Lawrence, A., Wilson, A. S., Elvis, M., & Wright, A. E. 1987, MNRAS, 228, 521
van Groningen, E., & Wanders, I. 1992, PASP, 104, 700
Véron-Cetty, M. P., Woltjer, L., & Roy, A. L. 1991, A&A, 246, L73
Wamsteker, W., & Colina, L. 1986, ApJ, 311, 617
Wanders, I., et al. 1993, A&A, 269, 39
Ward, M., Wilson, A. S., Penston, M. V., Elvis, M., Maccacaro, T., & Tritton, K. P. 1978, ApJ, 223, 788
White, R. J., & Peterson, B. M. 1994, PASP, 106, 879
Wilson, A. S., & Penston, M. V. 1979, ApJ, 232, 389
Winge, C., Peterson, B. M., Horne, K., Pogge, R. W., Pastoriza, M. G., & Storchi-Bergmann, T. 1995, ApJ, 445, 680 (Paper I)
Winkler, H. 1992, MNRAS, 257, 677
Winkler, H., Glass, I. S., van Wyk, F., Marang, F., Spencer Jones, J. H., Buckley, D. A. H., & Sekiguchi, K. 1992, MNRAS, 257, 659
Wolstencroft, R. D., Done, C. J., Scarrott, S. M., & Scarrott, R. M. J. 1995, MNRAS, 276, 460
Zdziarski, A. A., Fabian, A. C., Nandra, K., Celotti, A., Rees, M. J., Done, C., Coppi, P. S., & Madejski, G. M. 1994, MNRAS, 269, L55